Accepted Manuscript

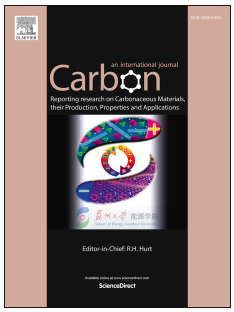

A comparative study of activated carbon aerogel and commercial activated carbons as electrode materials for organic electric double-layer capacitors

Inchan Yang, Dahye Kwon, Myung-Soo Kim, Ji Chul Jung

PII: S0008-6223(18)30206-9

DOI: 10.1016/j.carbon.2018.02.076

Reference: CARBON 12912

To appear in: *Carbon*

Received Date: 21 August 2017

Revised Date: 7 February 2018

Accepted Date: 18 February 2018

Please cite this article as: I. Yang, D. Kwon, M.-S. Kim, J.C. Jung, A comparative study of activated carbon aerogel and commercial activated carbons as electrode materials for organic electric double-layer capacitors, *Carbon* (2018), doi: 10.1016/j.carbon.2018.02.076.

Activated carbon aerogel (ACA)

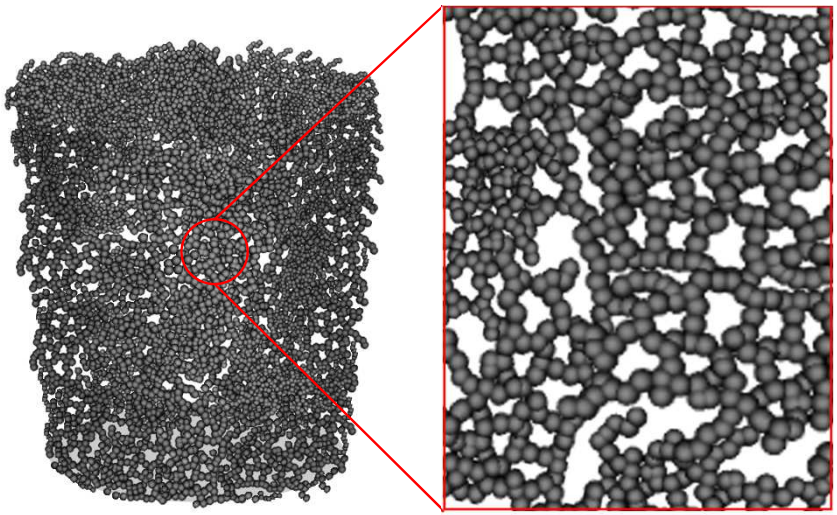

- 3D networking structure (**low electronic resistance**)
- Abundant mesopores (low ionic resistance)
- Abundant micropores (**high surface area**)

Electric double-layer capacitor

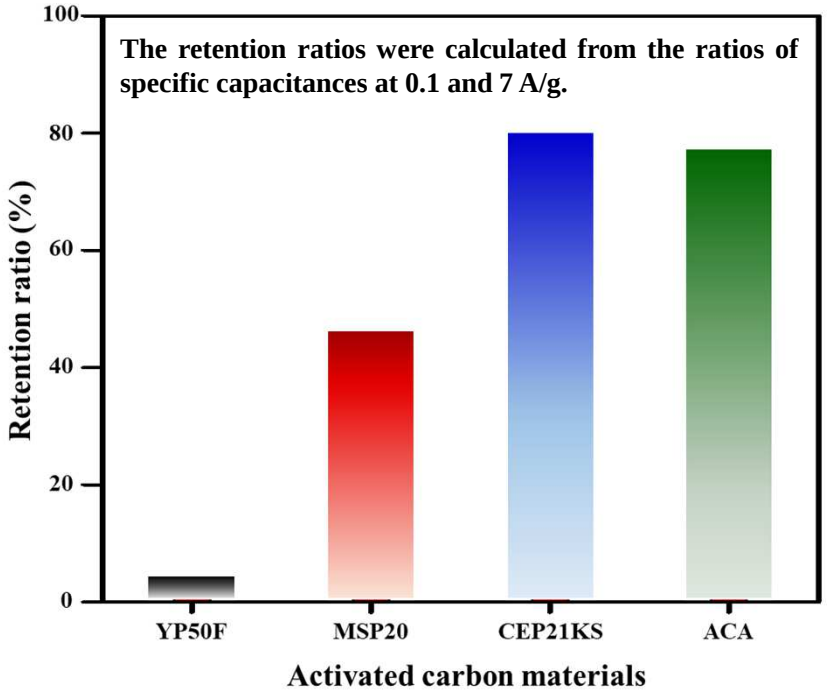

Carbon (CARBON-D-17-02948R2)

A comparative study of activated carbon aerogel and commercial activated carbons as electrode materials for organic electric double-layer capacitors

Inchan Yang, Dahye Kwon, Myung-Soo Kim, Ji Chul Jung*

Department of Chemical Engineering, Myongji University,
Yongin 17058, South Korea

*Corresponding author. Tel: +82-31-330-6390. E-mail: jcjung@mju.ac.kr (Ji Chul Jung)

Abstract

In this study, we thoroughly compared the electrochemical performances of activated carbon aerogel (ACA) and commercial activated carbons (CACs) as electrode materials for organic electric double-layer capacitors (EDLCs) to investigate the feasibility of ACA for commercial applications. The capacitive behavior of carbon materials as EDLC electrodes is strongly influenced by their specific surface areas and electronic resistances, which are determined by several preparation factors, including raw materials and activation methods. Unlike CACs, which have only micropores, ACA has both abundant micropores and mesopores, leading to a high surface area and low density. ACA also shows relatively low electronic resistance because of its three-dimensional structural features. Accordingly, ACA exhibits considerable capacitance at a low charge–discharge rate and excellent performance even at a high charge–discharge rate, indicating that ACA is a promising carbon material for organic EDLC electrodes. Furthermore, this comparison study clearly demonstrates that newly developed carbon materials for commercially advanced EDLC electrodes should exhibit both high specific surface area and low electronic resistance.

1. Introduction

Electric double-layer capacitors (EDLCs) have been intensively studied as electrical energy devices to complement or replace secondary batteries [1-5]. As EDLCs store electrical energy by forming Helmholtz double-layers at the interface between the electrode and electrolyte, EDLCs have many advantages, including fast discharge rates, durable life cycles, and high power densities [6]. Owing to these unique characteristics, EDLCs have received considerable attention as next-generation electrical energy devices and are already widely applied in various fields requiring short-term high currents [5,7].

EDLCs can be divided into three parts; an electrode, a separator, and an electrolyte. Most research for improving the electrochemical performances of EDLCs has been conducted on electrodes that generally comprise an active material [8-23], a conductive additive [24-26], and a binder [27]. Activated carbons that maximize the adsorption of electrolyte ions are typically used as the active material. Carbon blacks, which are commonly used as conductive additives in EDLC electrodes, are substances having excellent conductivity owing to the continuous connection of the carbon particles therein. Two types of binder, i.e., aqueous and non-aqueous, are used to bind an active material and a conductive additive. Polytetrafluorethylene (PTFE) is a typical aqueous binder, while polyvinylidene fluoride (PVDF) is a representative non-aqueous binder. However, most studies on EDLCs concentrate on active materials because their properties can directly affect the electrochemical performances of EDLCs. Pore-size control of active materials [28-30], activation methods that maximize specific surface areas [31-34], and imparting crystallinity to improve conductivity [35] are the main areas of interest in active-material research.

Activated carbons are the most commonly used active material for commercial EDLCs

because of their high specific surface areas, which are imparted by abundant micropores (<2 nm) [11-13]. High-grade commercial activated carbons (CACs) having specific surface areas of 1,500 m^2/g or more are most commonly applied to commercial EDLCs. The YP series (Kuraray Co., Japan), MSP20 (Kansai Coke & Chemicals Co., Japan), and the CEP series (Power Carbon Technology Co., Korea) are examples of high-grade CACs used for EDLC electrodes. Table 1 summarizes the properties of these CACs [36-38].

Most researchers agree that activated carbons with abundant pores providing large surface areas are advantageous as electrode materials for EDLCs. However, an abundance of pores can also be a disadvantage since it can cause decreased conductivity. Thus, abundant pores in activated carbons can be a conflicting property for EDLC electrodes, and several studies have been conducted recently to overcome this dichotomy [39-42]. Accordingly, not only activated carbons but also carbon nanotubes (CNTs) [14-17], graphene [18-20], and carbon aerogels (CAs) [21-23] are being researched as active materials for EDLCs. However, more studies on the commercial applicability of newly developed carbon materials are required as there are very few reports comparing the above-mentioned new carbon materials with CACs as active materials for EDLCs.

CAs, which exhibit low resistances owing to their three-dimensional (3D) networks of carbon particles, are becoming widely studied as active materials for EDLC electrodes [21-23,43,44]. Furthermore, CAs are good experimental materials for EDLC electrodes because their pore sizes can be systematically controlled by changing their preparation conditions. Therefore, there are numerous reports on methods of pore-size control for CAs and how their pore size is related to their electrochemical performance in EDLCs [29,30,45-47].

We have successfully conducted research on the synthesis of CAs for EDLCs [45-47]. Furthermore, through activation with KOH, we have synthesized activated carbon aerogels

(ACAs) with both large surface areas and good conductivities. In the present study, we thoroughly compare an ACA and several types of CAC prepared using different raw materials and activation methods for use as active materials for EDLC electrodes to assess the feasibility of the commercial application of ACAs. For this purpose, a number of characterizations and electrochemical performance measurements of different carbon materials were performed under the same experimental conditions. From the results, we investigated how the physical properties of the active materials influence their electrochemical properties, including the capacitances and resistances of the EDLCs they are employed in. Through comparison of several CACs and ACA, we have investigated the properties that should be considered for newly developed carbon materials for EDLC electrodes. We believe that this study will be of great help in the development and improvement of active materials for advanced EDLC electrodes.

Table 1. Properties of the commercial activated carbons.

	Maker	Activation method	Raw material	S_{BET} [a] (m^2/g)
YP50F	Kuraray Co., Japan	Physical activation by steam	Coconut shell (hard carbon)	ca. 1600 m^2/g [36]
MSP20	Kansai Coke & Chemicals Co., Japan	Chemical activation by KOH	Phenolic resin (hard carbon)	ca. 2300 m^2/g [37]
CEP21KS	Power Carbon Technology Co., Korea	Chemical activation by KOH	Cokes (soft carbon)	ca. 2050 m^2/g [38]

[a] Specific surface areas were confirmed by the references

2. Experimental

2.1. Preparation of activated carbon aerogel

Carbon aerogel was synthesized by polymerization of resorcinol ($C_6H_6O_2$, Sigma-Aldrich) and formaldehyde (H_2CO, Wako) in aqueous solution using sodium carbonate (Na_2CO_3, Sigma-Aldrich) as a base catalyst [43,44]. The molar ratio of resorcinol and formaldehyde was 1:2, and the molar ratio of resorcinol to catalyst was 500:1. The weight percent of reactants (resorcinol, formaldehyde, and sodium carbonate) in the aqueous solution was 40%, and the total volume of reactants was ca. 70 mL [45].

First, the aqueous solution in which all the reactants were dissolved was vigorously mixed using stirring at ambient temperature and pressure for 2 h. During this step, small clusters of resorcinol and formaldehyde compounds (RF clusters) were synthesized. After mixing for 2 h, the solution containing the RF clusters was thoroughly sealed in a vial and stored in a convection oven for 2 days at 80 °C. In this step, the RF clusters cross-link to form an RF gel having a 3D structure. Then, a solvent exchange process was conducted using fresh acetone every 3 h for 1 day to maintain 3D network structure of the RF gel. The resultant RF gel was then dried at room temperature for 1 day and 50 °C for 1 day. The CA was prepared by pyrolysis of the dried RF gel in a tube furnace at 800 °C for 2 h under nitrogen flow. After this step, the obtained CA was ground into a powder and passed through a 400-mesh sieve to obtain a fine CA powder.

ACA was prepared by the pyrolysis process of CA with potassium hydroxide (KOH, Daejung Chem). The CA and KOH were physically mixed at a mass ratio of 4:1 and pyrolyzed in a tube furnace at 800 °C for 2 h under flowing nitrogen. After pyrolysis, the ACA was thoroughly washed with distilled water and dried for 1 day to obtain a pure ACA

powder.

2.2. Characterization of activated carbon materials

To confirm the physical properties of prepared activated carbon materials (CACs and ACA), we performed N_2 adsorption/desorption isotherm analysis using a constant-volume adsorption apparatus (BELSORP-max, BEL Japan) at −196 °C. From the obtained results, the specific surface areas and related pore and volume properties were obtained [48]. The specific surface areas of the activated carbon materials were calculated using the Brunauer–Emmett–Teller (BET) equation. In addition, pore-size distributions were obtained using the Barrett–Joyner–Halenda (BJH) method and non-local density functional theory (NLDFT) [49].

2.3. Preparation of coin-type EDLC using activated carbon materials

EDLC electrodes were prepared using the CACs or the synthesized ACA, Super-P (M.M.M. Carbon Co., Belgium), and polyvinylidene fluoride (Sigma-Aldrich) dissolved in 1-methyl-2-pyrrolidone (NMP, Daejung Chem). An activated carbon material, Super-P, and PVDF were used as the active material, conductive additive, and binder, respectively. First, the active material and conductive additive were mixed using a ball-mill for 30 min. Then, the binder was added to the mixture and it was stirred for 1 h to obtain a homogeneous slurry. The weight ratio of the electrode materials was fixed 8:1:1 (active material:conductive additive:binder). The slurry was coated onto an aluminum current collector using a doctor blade with a gap of 22 μm. The coated electrode was then dried in a vacuum oven at 70 °C for 1 day and then pressed at 80 °C with a double roll-press. To fabricate coin-type EDLC cells, circular electrodes of 18-mm diameter were obtained by punching.

Coin-type CR2032-battery-size EDLCs were assembled using the prepared electrode, a separator, and a spacer. The electrodes and separator were soaked in an organic electrolyte (1 M tetraethylammonium tetrafluoroborate dissolved in acetonitrile ($TEABF_4$/ACN) for 12 h in a glovebox filled with nitrogen gas. After soaking, the separator was placed between the electrodes. Finally, the EDLC cell was sealed with a cell crimper (Wellcos Co.). This fabrication was also performed in a glove box filled with inert gas.

2.4. Electrochemical characterization of activated carbon materials

The electrochemical performances of the assembled coin-type EDLC cells were measured by cyclic voltammetry (CV; CS310, CorrTest), galvanostatic charge/discharge analysis (C/D; CS310, CorrTest), four-point probe measurement (FPP; CMT-SR1000N, Advanced Instrument Technology), and electrochemical impedance spectroscopy (EIS; CS310, CorrTest). To assess the charge–discharge behavior of the EDLCs, we analyzed the CV and C/D results. CV curves of the cells were taken at scan rates from 10 to 300 mV/s in the voltage range 0–2.7 V, and C/D measurement was conducted at constant current loads (0.1 to 7 A/g) in the same voltage range as that used for the CV measurements. The specific capacitances (gravimetric capacitance (C_g) and volumetric capacitance (C_v)) of the EDLC cells were calculated using the discharge curve from the C/D measurements. C_v of EDLC cells was obtained by multiplying C_g and density of electrode materials ($\rho_{electrode}$), which was determined from the ratio of loading mass to volume of electrode materials. To check the resistance properties of the assembled EDLC cells, FPP measurements were conducted to determine the electronic resistances directly, and Nyquist plots were obtained from EIS analysis over a frequency range of 100 kHz to 0.01 Hz to confirm charge-transfer resistance, which is influenced by electronic resistance and ionic resistance, of the CACs and ACA.

3. Results and discussion

3.1. Physical properties of activated carbon materials

To investigate the physical properties of the CACs and ACA, including specific surface areas, pore-size distributions, and pore volumes, nitrogen adsorption/desorption isotherms were measured. All experiments were conducted three times, and the average value was used as a result. The results are presented in Fig. 1 and Table 2.

YP50F is a CAC made from a natural raw material (coconut shell) using physical activation with steam. In comparison with the other CACs (MSP20 and CEP21KS) and ACA, YP50F has a relatively low specific surface area (Table 2 and Fig. 1(a)). In addition, YP50F has a considerable amount of impurities, as shown in Table S1 [13]. For these reasons, we assumed that the electrochemical properties of YP50F as an electrode material for EDLCs would be poor because of its poor adsorption of electrolyte ions (owing to its low surface area) and high electronic resistance (owing to impurities).

Unlike YP50F, MSP20 and CEP21KS exhibit high specific surface areas because they are made using KOH chemical activation, which is a more favorable method for synthesizing porous carbon materials than physical activation with steam (Table 2). Therefore, we expected that both MSP20 and CEP21KS would show better electrochemical performances than that of YP50F owing to their higher surface areas and lower resistances. Figure 1 and Table 2 confirm that the physical properties of MSP20 and CEP21KS are similar. However, we also assumed that there would be differences in their electrochemical properties as electrode materials for EDLCs owing to the difference in their raw materials. Particularly, the

resistance properties of MSP20 and CEP21KS were expected to be different because phenolic resin (which is a raw material for MSP20) is a hard carbon and coke (which is the raw material for CEP21KS) is a soft carbon. In previous research by our group, we confirmed that the resistance property of electrode materials has a significant effect on their capacitance properties under high-rate charge–discharge conditions [47]. In short, MSP20 and CEP21KS have similar physical properties, but we predicted that CEP21KS, which is made from soft carbon, would exhibit better capacitance properties than MSP20 under high-rate charge–discharge conditions because of differences in their resistance properties.

Like MSP20, ACA is synthesized from phenolic resin, but the physical properties of ACA are very different to those of MSP20 because of the structural features of ACA. ACA is known to have excellent conductivity and low resistance owing to its 3D network structure. As shown in Fig. 1(a), all the CACs exhibit typical I-type isotherms, while ACA exhibits an IV-type isotherm curve with H_2-type hysteresis. This means that, unlike the CACs, which have abundant micropores only, ACA contains a significant amount of mesopores as well as numerous micropores. This is confirmed more directly by the pore-size distribution diagrams (Fig. 1(b), (c)), which also show that ACA presents a large pore volume owing to its abundant mesopores. From the pore properties of ACA, we predicted that density of ACA would be lower than those of the CACs. Moreover, owing to its low density, although ACA shows the largest specific surface area, its actual surface area-to-volume ratio is not sufficiently large.

To summarize, YP50F was predicted to show the poorest electrochemical performance because it has the lowest specific surface area and high impurity levels. The physical properties of MSP20 and CEP21KS are very similar, but we predicted that their electrochemical properties would be different because of differences in their raw materials. The raw material for MSP20 is phenolic resin (hard carbon) and that for CEP21KS is coke

(soft carbon). Therefore, because of differences in the resistance properties owing to the different raw materials, we expected that CEP21KS would exhibit better capacitance properties than MSP20 under high-rate charge–discharge conditions, although the capacitance properties of MSP20 and CEP21KS are similar under low-rate charge–discharge conditions. In addition, through the physical properties of ACA (Fig. 1 and Table 2), we confirmed the successful formation of ACA, which was made from phenolic resin (like MSP20). However, although ACA and MSP20 are made from the same raw material, their physical properties are very different because of the 3D network structural features of ACA, which lead to low resistance. In addition, we concluded from its nitrogen adsorption–desorption isotherm curve and pore-size distribution measurements that ACA contains not only abundant micropores but also abundant mesopores. Therefore, we also expected that the capacitance properties of ACA under low-rate charge–discharge conditions would be maintained under high-rate charge–discharge conditions.

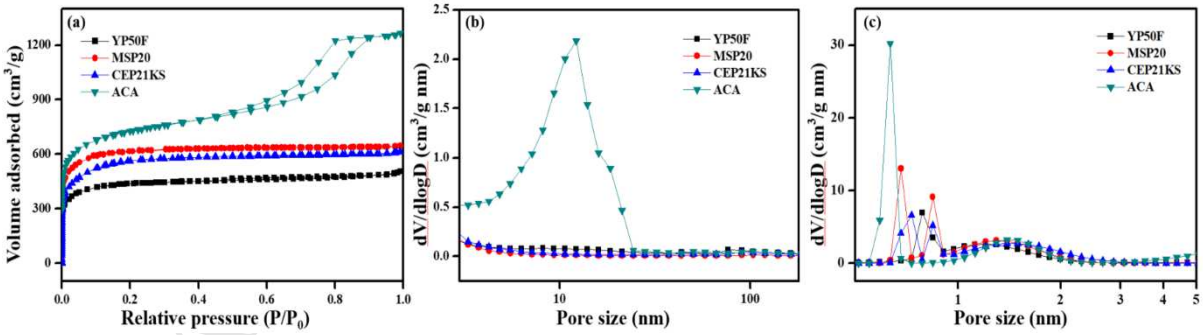

Fig. 1. (a) N_2 adsorption/desorption isotherms and pore size distributions of the activated carbon materials using (b) BJH and (c) NLDFT methods.

Table 2. Physical properties of commercial activated carbons (CACs) and activated carbon aerogel (ACA).

	S_{BET} [a] (m^2/g)	$D_{avg.}$ [b] (nm)	V_{micro} [c] (cm^3/g)	V_{meso} [d] (cm^3/g)	V_{total} [e] (cm^3/g)
YP50F	1590	1.8	0.7	0.2	0.8
MSP20	2330	1.8	1.0	0.1	1.0
CEP21KS	2090	1.9	1.0	0.1	1.1
ACA	2690	2.9	0.6	1.1	2.0

[a] Specific surface area: calculated by the Brunauer-Emmett-Teller (BET) plot

[b] Average pore diameter: determined by the Barret-Joyner-Hallender (BJH) method with the desorption branch

[c] Micropore volume

[d] Mesopore volume

[e] Total pore volume

3.2. Capacitance properties of activated carbon materials

Before discussing the capacitance performances of the activated carbon materials as EDLC electrode materials, we will first describe some of the differences between the two-electrode system (2E) and three-electrode system (3E) for understanding the capacitance properties of EDLC cells used in this report. Although the majority of researchers apply the 3E system, this study used the 2E system to measure the capacitances of the EDLC cells. This is because the organic electrolyte $TEABF_4$/ACN, which is similar to that used in most commercial full-cell-type EDLCs, was applied. Thus, using the 2E system would have more industrial worth than using the 3E system. In addition, it is more appropriate to apply 2E than 3E because our aim is to compare CACs and ACA as EDLC electrodes. Assuming that each

EDLC electrode employed has the same weight, the following equation relates the specific capacitances determined using 3E and 2E EDLCs [50]:

$$C_{3E} = 4 \times C_{2E}, \quad (1)$$

Where C is the specific capacitance. Therefore, Eq. 1 should be used to analyze the capacitance properties determined using the 3E system. In this study, we successfully configured a 2E system for measuring the electrochemical performances of the activated carbon materials (CACs and ACA) as organic EDLC electrode materials.

The cyclic voltammograms for the CACs and ACA at various scan rates (10–300 mV/s) are shown in Fig. 2. MSP20 shows the largest CV area at a low scan rate (10 mV/s), while the CV areas of CEP21KS and ACA are larger than that of MSP20 at a high scan rate (300 mV/s). Moreover, CEP21KS and ACA show a fairly well-maintained rectangular shape at a high scan rate of 300 mV/s. In addition, YP50F presents a CV area similar to that of ACA at 10 mV/s, but it rapidly decreases as the scan rate increases. From these trends, we can infer that MSP20 has the highest specific capacitance for the low-rate charge–discharge process, but the specific capacitances of CEP21KS and ACA are higher than that of MSP20 for the high-rate charge–discharge process. Moreover, we can also predict the trend for the electronic resistances of the CACs and ACA because the CV area for the high-rate charge–discharge rate process is influenced by electronic resistance. In other words, by comparing the CV areas of the CACs and ACA at a high scan rate, we can predict that the order of resistance for the CACs and ACA would be YP50F > MSP20 > ACA > CEP21KS.

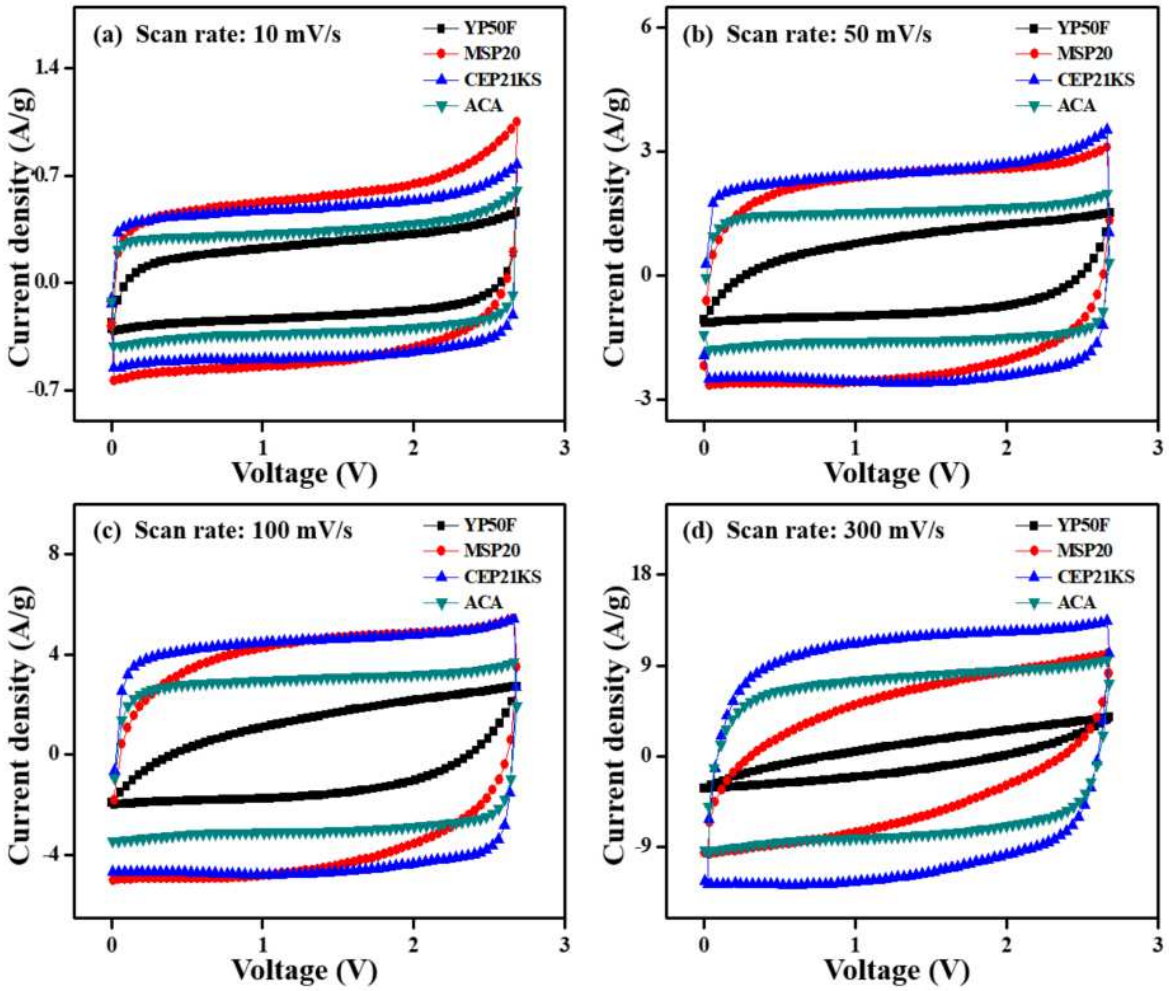

Fig. 2. Cyclic voltammograms of the activated carbon materials at a scan rate of (a) 10 mV/s, (b) 50 mV/s, (c) 100 mV/s, and (d) 300 mV/s.

To compare the capacitance properties of the applied activated carbon materials for EDLC electrodes, we also performed C/D measurements. Fig. 3 shows the C/D curves obtained at different current densities (0.1–7 A/g). In addition, we determined the C_g of the EDLCs with CACs and ACA as the electrode materials in accordance with the following equation:

$$C_g = \frac{I \cdot \Delta t}{m \cdot \Delta V}, \quad (2)$$

where C_g is the gravimetric capacitance, C_v is the volumetric capacitance, I is the discharge current, Δt is the time for discharge, m is the weight of the two electrode materials, ΔV is the change in voltage during discharge. For commercial application of EDLCs, volumetric capacitance is also important along with gravimetric capacitance. Accordingly, we calculated the C_v of the CACs and ACA electrodes using the following equation:

$$C_v = C_g \times \rho_{electrode} , \quad (3)$$

where $\rho_{electrode}$ is density of electrode materials determined from the ratio of loading mass to volume of electrode materials. For this calculation, we also summarized the loading mass of active materials (CACs and ACA) and electrode thickness in Table 3.

The obtained gravimetric and volumetric capacitances are presented in Table 4 and 5, respectively, and diagrams showing the trend in capacitance with charge–discharge rate are shown in Fig. 4. To compare the specific capacitances of CACs and ACA, we also calculated the retention ratios of capacitance with increasing charge–discharge rate (Table 4 and 5). The retention ratios of the EDLC cells were calculated from the ratios of specific capacitances at 0.1 and 7 A/g.

The C/D profiles (Fig. 3) show that activated carbon materials with large surface areas exhibit high capacitances at low current densities (low-rate charge–discharge process). Although ACA shows the largest specific surface area (Table 2), we inferred that the large value for the specific surface area of ACA is due to its low density, as previously described. In other words, the surface-area-to-volume ratios of MSP20 and CEP21KS are larger than that of ACA because of the low density of ACA, resulting from its abundant mesopores. Therefore, under low-rate charge–discharge conditions (0.5 and 1 A/g), MSP20 and CEP21KS show longer discharge times than that of ACA. With increasing charge–discharge

rate, however, the discharge time of MSP20 rapidly decreases. At current densities of 5 and 7 A/g, the discharge times ACA and CEP21KS are longer than that for MSP20. This reversal in the trend of capacitances at high current density (high-rate charge–discharge process) is consistent with the trend for the CV areas. Using these results, we could also predict the same order for the electronic resistances as that obtained from the CV area results. The specific capacitances of CACs and ACA with changing current density are presented in Fig. 4. As expected, MSP20 exhibits high values for specific capacitance at 0.1 and 0.5 A/g, but the gravimetric capacitances of CEP21KS and ACA are even higher than those of MSP20 at 5 and 7 A/g. In addition, the discharge times for YP50F are the shortest at all charge–discharge rates. In particular, at a current density of 3 A/g or more, the specific capacitances of YP50F are very poor in comparison with those of the other carbon materials. The retention ratios as changes in charge–discharge rate, which were calculated from the ratio of specific capacitances at 0.1 and 7 A/g, are also presented in Table 4 and 5. Through these results, we confirm that the retention ratios decrease in the order CEP21KS > ACA > MSP20 > YP50F. This order is also in good agreement with the order of CV areas and the capacitance properties of CACs and ACA under high-rate charge–discharge conditions.

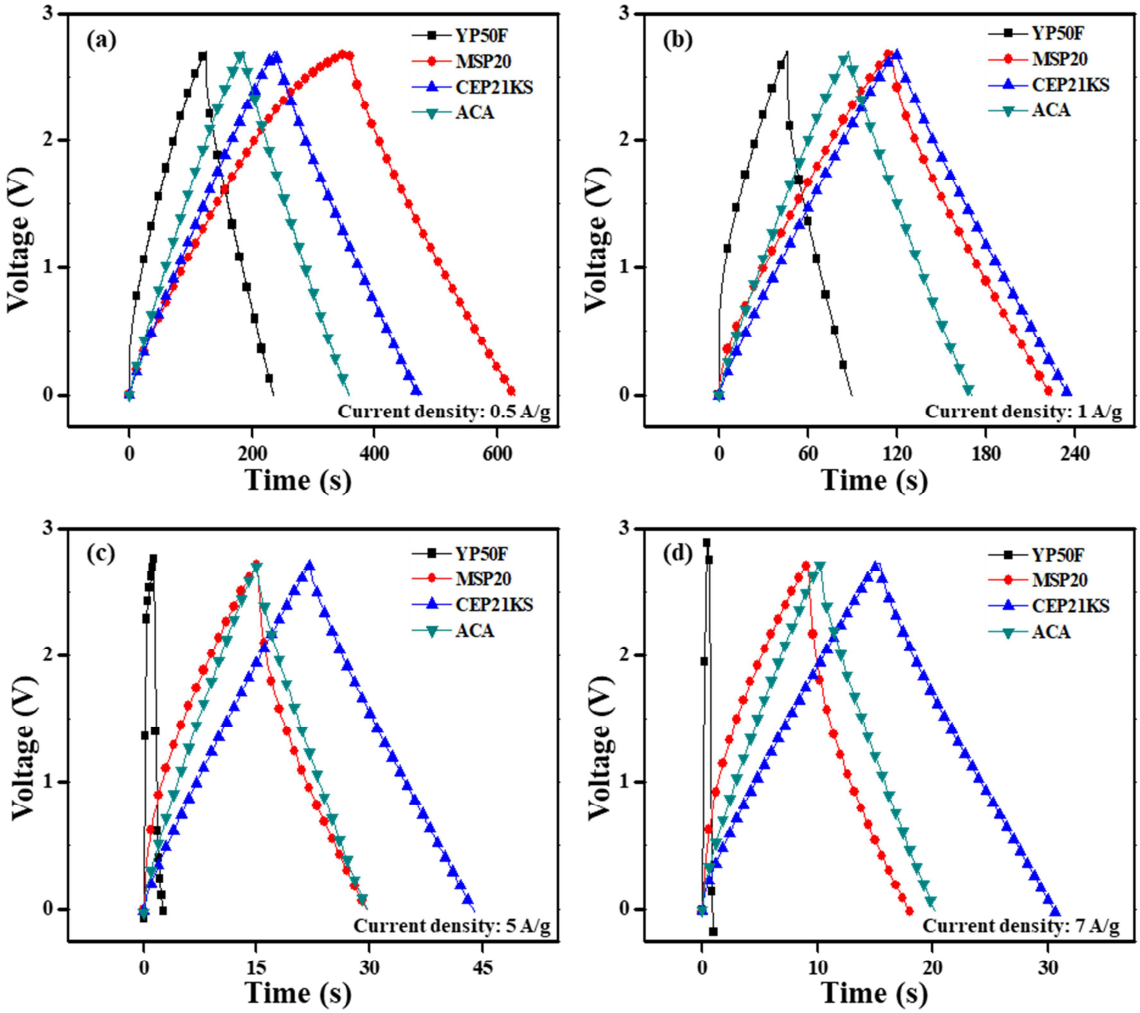

Fig. 3. Galvanostatic charge/discharge profiles of the activated carbon materials at a constant current density of (a) 0.5 A/g, (b) 1 A/g, (c) 5 A/g, and (d) 7 A/g.

1 **Table 3. Loading mass of active material and electrode thickness.**

	Loading mass of active material (mg/cm^2)	Electrode thickness[a] (μm)
YP50F	0.66	39
MSP20	0.57	40
CEP21KS	0.61	38
ACA	0.49	40

2 [a] Electrode thickness includes the thickness of current collector (20 μm)

Table 4. Gravimetric capacitance and retention ratio of the activated carbon materials calculated from C/D profiles.

	Gravimetric capacitance (F/g)						
Current density (A/g)	0.1	0.5	1	3	5	7	R_{ret} [a]
YP50F	24	20	16	6	2	1	0.04
MSP20	50	50	40	32	27	23	0.46
CEP21KS	48	43	43	41	40	39	0.81
ACA	33	32	30	28	27	26	0.79

[a] Retention ratio with increasing charge-discharge rate: calculated from the ratio of specific capacitances at 0.1 and 7 A/g

Table 5. Volumetric capacitance and retention ratio of the activated carbon materials calculated from C/D profiles.

	Volumetric capacitance (F/cm^3)						
Current density (A/g)	0.1	0.5	1	3	5	7	R_{ret} [a]
YP50F	10	9	7	3	1	0	0
MSP20	18	18	14	11	10	8	0.44
CEP21KS	20	18	18	17	17	17	0.85
ACA	10	10	9	9	8	8	0.80

[a] Retention ratio with increasing charge-discharge rate: calculated from the ratio of specific capacitances at 0.1 and 7 A/g

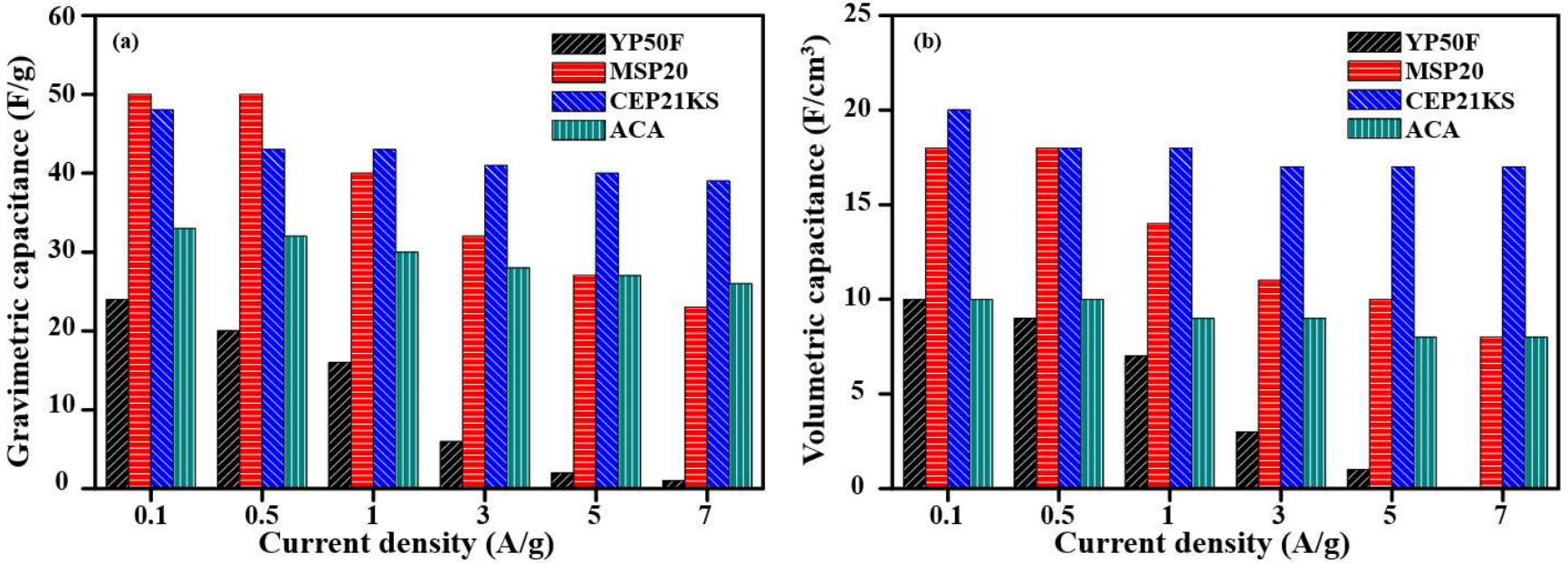

Fig. 4. Specific capacitance of the activated carbon materials with respect to current density ((a) gravimetric capacitance and (b) volumetric capacitance).

3.3. Resistance properties of activated carbon materials

From the physical and capacitance properties of the activated carbon materials, we inferred that the high capacitance properties under high-rate charge–discharge conditions are due to the low resistance properties of the electrode material. To verify this inference, we conducted FPP measurement, which is a method used to assess the sheet resistance of a thin film. We also used EIS analysis to determine the charge-transfer resistance (R_{ct}), which is influenced by electronic resistance and ionic resistance. The results of the FPP measurements are presented in Table 6, and the results of the EIS analysis are shown in Fig. 5 with the Nyquist plots.

From the sheet resistance results for the CACs and ACA (Table 6), we confirm that the order of electronic resistances for the activated carbons is consistent with our prediction. YP50F shows the highest value of sheet resistance. CEP21KS, which is made from soft carbon (coke), and ACA, which is known to exhibit low resistance owing to its 3D network structure, exhibit relatively low values for sheet resistance. The sheet resistance of MSP20, which is made from phenolic resin like ACA, is lower than that of YP50F but higher than that of ACA.

Prior to discussing the resistance performances of EDLC cells with CACs and ACA, we first explain the use of Nyquist plots from EIS measurements to understand resistance properties. The Nyquist plots for EDLC cells can be explained in terms of three regions according to frequency. The first resistance in the Nyquist plot is the bulk solution resistance (R_s), which can be obtained from the *x*-intercept in the highest-frequency region. R_s is dictated by the electrolyte solution used for the EDLC cells. In the middle-frequency region, the charge-transfer resistance (R_{ct}) is obtained from the semicircle loop, and it is influenced by ionic and electronic resistances. Ionic resistance is related to the mobility of electrolyte

ions in the interparticle pores, and electronic resistance is determined by the conductivity of the electrode material and the contact resistance between the electrode material and the current collector. The R_{ct} values for electrode materials are of particular interest to researchers working in the field of EDLC electrodes. Lastly, the Warburg response, which appears as a curved line observed in the low-frequency region, results from ion transport processes in the intraparticle pores of the electrode, which mostly consist of micropores [51,52]. In this study, the semicircle loop, which is closely related to the R_{ct}, is very important because it is the region where we obtain the relationship between the change in capacitance properties depending on charge–discharge rate (described in the previous section) and the resistance properties.

As shown in Fig 5, the order of the semicircle loop radii for the activated carbon materials is similar to the order of electronic resistances. The radii of the semicircles decrease in order YP50F > MSP20 > CEP21KS > ACA. In other words, YP50F shows the highest charge-transfer resistance and ACA shows the lowest. The order of the charge-transfer resistances for the CACs and ACA does not match with the order of electronic resistances obtained from FPP measurements, which indicated that CEP21KS has the lowest electronic resistance. The reason for this mismatch is attributed to the charge-transfer resistance being influenced not only by electronic resistance but also by ionic resistance. Therefore, although ACA shows a higher electronic resistance than that of CEP21KS, ACA exhibits lower charge-transfer resistance than that of CEP21KS because ACA has a low ionic resistance owing to its abundant mesopores. From this mismatch, we also confirm that capacitance properties of EDLC cells under high-rate charge–discharge conditions are more influenced by electronic resistance than ionic resistance.

In summary, we conducted FPP measurements and EIS analysis to investigate the

resistance properties of CACs and ACA. Through the FPP results, we verified the order of the electronic resistances of the activated carbon materials. The electronic resistance is in order YP50F > MSP20 > ACA > CEP21KS. This order of electronic resistances matches with the order of resistances predicted from physical and capacitance properties. However, in the results from EIS, the order of charge-transfer resistances does not match with that for electronic resistances derived from FPP because charge-transfer resistance is influenced by ionic as well as electronic resistance. Therefore, ACA, which has abundant mesopores, exhibits the lowest charge-transfer resistance owing to its low ionic resistance. The order of charge-transfer resistances is in the order YP50F > MSP20 > CEP21KS > ACA. However, considering the capacitance properties of the CACs and ACA, we conclude that the capacitance properties of EDLCs under high-rate charge–discharge conditions are more influenced by the electronic resistance than by the ionic resistance of the electrode materials.

Table 6. Sheet resistance of the activated carbon materials.

Activated carbon materials	YP50F	MSP20	CEP21KS	ACA
R_{sheet} [a]	1504.0	442.9	281.0	377.8

[a] Sheet resistance: confirmed by four-point probe measurement

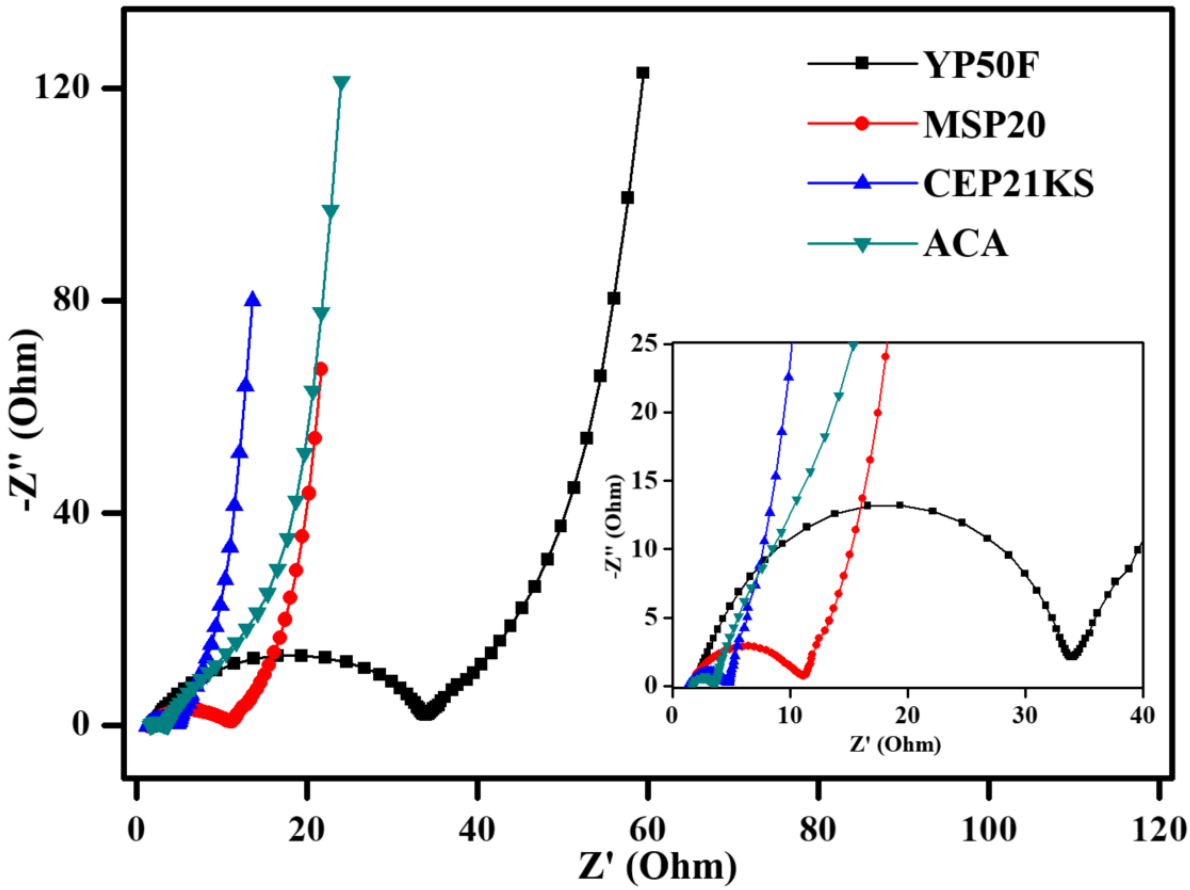

Fig. 5. Nyquist plots of the activated carbon materials.

3.4. Relationships between physical properties and electrochemical properties

The results so far indicate that there are crucial relationships between the physical properties of the activated carbon materials and the capacitance and resistance properties of their corresponding EDLCs.

YP50F is a CAC made from coconut material that is physically activated using steam. Therefore, we assumed that the purity of YP50F would be poor, leading to high electrical resistance. Moreover, we also predicted that the capacitance properties of YP50F would be poor because it has a smaller surface area compared with those of the other CACs (MSP20 and CEP21KS) and ACA owing to the fact that it is activated using a physical rather than a chemical method. We also predicted that the difference in raw materials used to make MSP20

and CEP21KS would have a significant effect on their electrochemical performances. MSP20 is made from synthesized phenolic resin, which is a hard carbon, and CEP21KS is made from purified coke, which is a soft carbon. Therefore, we expected that the electronic resistance of CEP21KS would be lower than that of MSP20, leading to a difference in the capacitance properties of MSP20 and CEP21KS. ACA is made from phenolic resin using a KOH activation method, like MSP20. However, ACA has abundant mesopores and low resistance owing to its 3D network structural features, unlike MSP20. Therefore, we predicted that ACA and MSP20 would exhibit different electrochemical behaviors as EDLC electrode materials.

As shown in Fig. 1 and Table 2, all the CACs (YP50F, MSP20, and CEP21KS) show I-type nitrogen adsorption/desorption isotherm curves, indicating that they have abundant micropores only. YP50F shows the smallest specific surface area, as we expected, and the specific surface areas of MSP20 and CEP21KS are larger than that of YP50F. This means that the pores in YP50F, which are formed by physical activation with steam, are not as well developed as those in MSP20 and CEP21KS, which are formed using chemical activation with KOH. Unlike the CACs, ACA shows abundant mesopores and thus has the largest specific surface area, as shown in Fig. 1 and Table 2.

From the capacitance properties of CACs and ACA (Fig. 2–4 and Table 4 and 5), we confirm that YP50F exhibits the worst capacitance properties under all charge–discharge rates. Moreover, with increasing charge–discharge rate, the capacitance properties of YP50F rapidly decrease. Therefore, YP50F is relatively unsuitable for EDLCs because their capacitance properties are greatly influenced by the resistance properties of the electrode material. In other words, the poor capacitance properties of EDLCs prepared with YP50F come from its poor physical properties and high resistance. By comparing MSP20 and CEP21KS, which show similar physical properties, we also confirmed the influence of the resistance properties

of the electrode materials on the capacitance properties of the corresponding EDLCs under high-rate charge–discharge conditions. Since the raw material for MSP20 is a hard carbon (phenolic resin) and that for CEP21KS is a soft carbon (coke), we assumed that their resistance properties would be different. Although both MSP20 and CEP21KS show high specific capacitances under low-rate charge–discharge conditions, the capacitance properties of MSP20 drastically decrease with increasing charge–discharge rate. Conversely, the capacitance properties of CEP21KS are well maintained under high-rate charge–discharge conditions. We assume that this difference in the capacitance properties of MSP20 and CEP21KS is also due to their resistance differences. ACA shows considerable capacitance properties under low-rate charge–discharge conditions. As shown in Table 4 and 5, moreover, ACA maintains its capacitance properties under high-rate charge–discharge conditions. In particular, the retention ratio for ACA is high, similarly to that of CEP21KS. We assume that the high retention ratio of ACA is due to its low resistance properties, which originate from its 3D network structural features.

In short, YP50F has a low specific surface area and thus shows the worst capacitance properties at all charge–discharge rates. MSP20 and CEP21KS made from hard carbon (phenolic resin) and soft carbon (coke), respectively, exhibit high capacitance properties under low-rate charge–discharge conditions. However, the capacitance properties of MSP20 rapidly decrease with increasing charge–discharge rate, while those of CEP21KS are maintained under high-rate charge–discharge conditions. ACA, with its 3D network structure that imparts low resistance, exhibits a good retention ratio. Thus, we conclude that the order of resistance for the CACs and ACA is YP50F > MSP20 > ACA > CEP21KS.

As shown in Table 6, the order of electronic resistance is YP50F > MSP20 > ACA > CEP21KS, as we predicted from the physical and capacitance properties of the CACs and

ACA. As shown in Fig. 5, however, the order of semicircle radii in the Nyquist plots, which are determined by charge-transfer resistance, decreases in the order YP50F > MSP20 > CEP21KS > ACA. This order mismatches with that derived from FPP measurements; this is because the radii of Nyquist plots are influenced by ionic resistance as well as electronic resistance.

ACA, which has good ionic resistance owing to its abundant mesopores, exhibits lower charge-transfer resistance than those of the CACs, which have micropores only, although the electronic resistance of ACA is higher than that of CEP21KS. Moreover, from the capacitance properties of the CACs and ACA under high-rate charge–discharge conditions, we confirm that the electronic resistance of an electrode material is a more important factor than its ionic resistance. In this study, therefore, we conclude that electrode materials with high specific surface areas can be used to make EDLCs that exhibit high capacitance performance at low charge–discharge rates, but EDLCs for high-rate charge–discharge rates should comprise electrode materials with not only high surface areas but also low electronic resistances. Moreover, we conclude that methods for synthesizing carbon electrode materials with both high surface areas and low electronic resistances are required for advanced EDLC electrodes.

4. Conclusions

The capacitive behaviors of ACA and CACs for EDLC electrodes were compared under the same experimental conditions with the aim of investigating the feasibility of the commercial application of ACA. For this purpose, three types of commercially available CACs (YP50F, MSP20, and CEP21KS) were purchased and ACA was synthesized by

polymerization of a resorcinol and formaldehyde, followed by chemical activation with KOH. At low charge–discharge rates, MSP20, CEP21KS, and ACA show considerable capacitance because of their high specific surface areas. As the charge–discharge rate increases, however, the capacitance of MSP20 drastically decreases, while CEP21KS and ACA maintain their good electrochemical performance. Various characterizations clearly revealed that the high specific surface area of a carbon material leads to high capacitance at low charge–discharge rates, while capacitive behavior at high charge–discharge rates is strongly affected by both specific surface area and electronic resistance. Accordingly, ACA, which has both abundant micropores and mesopores, exhibits considerable electrochemical performance at all charge–discharge rates due to its considerable specific surface area and low resistance, indicating the feasibility of the commercial application of ACA for advanced EDLC electrodes. In addition, we conclude that methods for preparing carbon materials with both high surface areas and low electric resistances, particularly electronic resistances, are required for advanced EDLC electrodes.

Acknowledgements

This work was supported by 2017 Research Fund of Myongji University.

References

[1] Wang G, Zhang S, Zhang J. A review of electrode materials for electrochemical supercapacitors. Chem Soc Rev 2012;41;797-828.

[2] González A, Goikolea E, Barrena JA, Mysyk R. Review on supercapacitors: Technologies and materials. Renew Sustain Energy Rev 2016;58;1189-206.

[3] Burt R, Birkett G, Zhao XS. A review of molecular modelling of electric double layer capacitors. Phys Chem Chem Phys 2014;16;6519-38.

[4] Sato T, Marukane S, Morinaga T, Kamijo T, Arafune H, Tsujii Y. High voltage electric double layer capacitor using a novel solid-state polymer electrolyte. J Power Sources 2015;295;108-16.

[5] Burke A. Ultracapacitors: why, how, and where is the technology. J Power Sources 2000;91;37-50.

[6] Belhachemi F, Raël S, Davat B. A physical based model of power electric double-layer supercapacitors. Industry Appl Conf 2000;5;3069-76.

[7] Miller JR, Simon P. Electrochemical capacitors for energy management. Science 2008;321;651-2.

[8] Jhang LL, Zhao XS. Carbon-based materials as supercapacitor electrodes. Chem Soc Rev 2009;38;2520-31.

[9] Yu Z, Tetard L, Zhai L, Thomas J. Supercapacitor electrode materials: nanostructures from 0 to 3 dimensions. Energy Environ Sci 2015;8;702-30.

[10] Simon P, Gogotsi Y. Materials for electrochemical capacitors. Nat Mater 2008;7;845-54.

[11] Gamby J, Teberna PL, Simon P, Fauvarque JF, Chesneau M. Studies and characterisations of various activated carbons used for carbon/carbon supercapacitors. J Power Sources 2001;101;109-16.

[12] Wei L, Yushin G. Nanostructured activated carbons from natural precursors for electrical double layer capacitors. Nano Energy 2012;1;552-65.

[13] Kim J-A, Park I-S, Seo J-H, Lee J-J. A development of high power activated carbon using the KOH activation of soft carbon series cokes. Trans Electr Electron Mater 2014;15;81-6.

[14] An KH, Kim WS, Park YS, Choi YC, Lee SM, Chung DC. Supercapacitors using single-walled carbon nanotube electrodes. Adv Mater 2001;13;497-500.

[15] Rangom Y, Tang X, Nazar LF. Carbon nanotube-based supercapacitors with excellent ac line filtering and rate capability *via* improved interfacial impedance. ACS Nano 2015;9;7248-55.

[16] Frackowiak E, Metenier K, Bertagna V, Béguin F. Supercapacitor electrode from multiwalled carbon nanotubes. Appl Phys Lett2000;77;2421-3.

[17] Venugopal N, Kim W. New α-$Zn_2V_2O_7$/carbon nanotube nanocomposite for supercapacitors. Korean J Chem Eng 2015;32;1918-23.

[18] Liu C, Yu Z, Neff D, Zhamu A, Jang BZ. Graphene-based supercapacitor with an ultrahigh energy density. Nano Lett 2010;10;4863-8.

[19] Wang Y, Shi Z, Huang Y, Ma Y, Wang C, Chen M. Supercapacitor devices based on graphene materials. J Phys Chem C 2009;113;13103-7.

[20] Miller JR, Outlaw RA, Holloway BC. Graphene electric double layer capacitor with ultra-high-power performance. Electrochim Acta 2011;56;10443-9.

[21] Biener J, Stadermann M, Suss M, Worsley MA, Biener MM, Rose KA. Advanced carbon aerogels for energy applications. Energy Environ Sci 2011;4;656-67.

[22] Halama A, Szubzda B, Pasciak G. Carbon aerogels as electrode material for electrical double layer supercapacitors-Synthesis and properties. Electrochim Acta 2010;55;7501-5.

[23] Kim CHJ, Zhao D, Lee G, Liu J. Strong, machinable carbon aerogels for high

performance supercapacitors. Adv Funct Mater 2016;26;4976-83.

[24] Jäckel N, Weingarth D, Zeiger M, Aslan M, Grobelsek I, Presser V. Comparison of carbon onions and carbon blacks as conductive additives for carbon supercapacitors in organic electrolytes. J Power Sources 2014;272;1122-33.

[25] Michael MS, Prabaharan SRS. High voltage electrochemical double layer capacitors using conductive carbons as additives. J Power Sources 2004;136;250-6.

[26] Yang I, Lee G, Jung JC. Effect of conductive additive amount on electrochemical performances of organic supercapacitors. Korean J Mater Res 2016;26;696-703.

[27] Abbas Q, Pajak D, Frąckowiak E, Béguin F. Effect of binder on the performance of carbon/carbon symmetric capacitors in salt aqueous electrolyte. Electrochim Acta 2014;140;132-8.

[28] Chmiola J, Yushin G, Gogotsi Y, Portet C, Simon P, Taberna PL. Anomalous increase in Carbon Capacitance at Pore Sizes Less Than 1 Nanometer. Science 2006;313;1760-3.

[29] Hamano Y, Tsujimura S, Shirai O, Kano K. Control of the pore size distribution of carbon cryogels by pH adjustment of catalyst solutions. Mater Lett 2014;128;191-4.

[30] Taylor SJ, Haw MD, Sefcik J, Fletcher AJ. Gelation mechanism of resorcinol-formaldehyde gels investigated by dynamic light scattering. Langmuir 2014;30;10231-40.

[31] Mitani S, Lee S-I, Yoon S-H, Korai Y, Mochida I. Activation of raw pitch coke with alkali hydroxide to prepare high performance carbon for electric double layer capacitor. J Power Sources 2004;133;298-301.

[32] Mitani S, Lee S-I, Saito K, Yoon S-H, Korai Y, Mochida I. Activation of coal tar derived needle coke with K_2CO_3 into an active carbon of low surface area and its performance as unique electrode of electric double-layer capacitor. Carbon 2005;43;2960-7.

[33] Kierzek K, Frackowiak E, Lota G, Gryglewicz G, Machnikowski J. Electrochemical capacitors based on highly porous carbons prepared by KOH activation. Electrochim Acta

2004;49;15-23.

[34] Frackowiak E, Delpeux S, Jurewicz K, Szostak K, Cazorla-Aoros D, Béguin F. Enhanced capacitance of carbon nanotubes through chemical activation. Chem Phys Lett 2002;361;35-43.

[35] Futaba DN, Hata K, Yamada T, Hiraoka T, Hayamizu Y, Kakudate Y. Shape-engineerable and highly densely packed single-walled carbon nanotubes and their application as super-capacitor electrodes. Nature Mater 2006;5;987-94.

[36] Zhang C, Hatzell KB, Boota M, Kyatkin B, Beidaghi M, Qiao W. Highly porous carbon spheres for electrochemical capacitors and capacitive flowable suspension electrodes. Carbon 2014;77:155-64.

[37] Kim T, Yoon Jeyong. Relationship between capacitance of activated carbon composite electrodes measured at a low electrolyte concentration and their desalination performance in capacitive deionization. J Electroanal Chem 2013;704:169-74.

[38] Shin H, Agostini M, Belharouak I, Hassoun J, Sun Y. High-power lithium polysulfide-carbon battery. Carbon 2016;96:125-30.

[39] Tao Y, Xie X, Lv W, Tang D-M, Kong D, Huang Z. Towards ultrahigh volumetric capacitance: graphene derived highly dense but porous carbons for supercapacitors. Sci Rep 2013;3;2975-82.

[40] Wang Q, Yan J, Fan Z. Carbon materials for high volumetric performance supercapaitors: design, challenges and opportunities. Energy Environ Sci 2016;9;729-62.

[41] Zhang L, Zhang F, Yang X, Long G, Wu Y, Zhang T. Porous 3D graphene-based bulk materials with exceptional high surface area and excellent conductivity for supercapacitors. Sci Rep 2013;3;1408-16.

[42] Zhang LL, Zhao X, Stoller MD, Zhu Y, Ji H, Murali S. Highly conductive and porous activated reduced graphene oxide films for high-power supercapacitors. Nano Lett

2012;12;1806-12.

[43] Pekala RW. Organic aerogels from the polycondensation of resorcinol with formaldehyde. J Mater Sci 1989;24;3221-7.

[44] Tamon H, Ishizaka H, Mikami M, Okazaki M. Porous structure of organic and carbon aerogels synthesized by sol-gel polycondensation of resorcinol with formaldehyde. Carbon 1997;35;791-6.

[45] Lee YJ, Jung JC, Yi J, Baeck S-H, Yoon JR, Song IK. Preparation of carbon aerogel in ambient conditions for electrical double-layer capacitor. Curr Appl Phys 2010;10;682-6.

[46] Yang I, Kim S-G, Kwon SH, Lee JH, Kim M-S, Jung JC. Pore size-controlled carbon aerogels for EDLC electrodes in organic electrolytes. Curr Appl Phys 2016;16;665-72.

[47] Yang I, Kim S-G, Kwon SH, Kim M-S, Jung JC. Relationships between pore size and charge transfer resistance of carbon aerogels for organic electric double-layer capacitor electrodes. Electrochim Acta 2017;223;21-30.

[48] Brunauer S, Emmett PH, Teller E. Adsorption of gases in multimolecular layers. J Am Chem Soc 1938;60;309-19.

[49] Barrett EP, Joyner LG, Halenda PP. The determination of pore volume and area distributions in porous substances. I. computations from nitrogen isotherms. J Am Chem Soc 195173;373-80.

[50] Qu D, Shi H. Studies of activated carbons used in double-layer capacitors. J Power Sources 1998;74;99-107.

[51] Yoo HD, Jang JH, Ryu JH, Park Y, Oh SM. Impedance analysis of porous carbon electrodes to predict rate capability of electric double-layer capacitors. J Power Sources 2014;267;411-20.

[52] Lei C, Markoulidis F, Ashitaka Z, Lekakou C. Reduction of porous carbon/Al contact resistance for an electric double-layer capacitor (EDLC). Electrochim Acta 2013;92;183-7.